SUPPLEMENTARY INFORMATION

Observation of polarization singularities and topological textures in sound waves

Ruben D. Muelas-Hurtado,[1,2] Karen Volke-Sepúlveda,[3] Joao L. Ealo,[2,4]
Franco Nori,[5,6] Miguel A. Alonso,[7,8] Konstantin Y. Bliokh,[5] and Etienne Brasselet[9]

[1]*School of Civil and Geomatic Engineering, Universidad del Valle, 760032 Cali, Colombia*
[2]*School of Mechanical Engineering, Universidad del Valle, 760032 Cali, Colombia*
[3]*Instituto de Física, Universidad Nacional Autónoma de México, Cd. de México, C.P. 04510, México*
[4]*Centro de Investigación e Innovación en Bioinformática y Fotónica, Universidad del Valle, 760032 Cali, Colombia*
[5]*Theoretical Quantum Physics Laboratory, RIKEN Cluster for Pioneering Research, Wako-shi, Saitama 351-0198, Japan*
[6]*Physics Department, University of Michigan, Ann Arbor, Michigan 48109-1040, USA*
[7]*Aix Marseille Univ, CNRS, Centrale Marseille, Institut Fresnel, Marseille, France*
[8]*The Institute of Optics, University of Rochester, Rochester, New York 14627, USA*
[9]*Univ. Bordeaux, CNRS, LOMA, UMR 5798, F-33400 Talence, France*

1. ℓ-dependent $\bar{S}_z$ for Bessel vortex fields

The figure S1 shows experimental and simulated dependence of the longitudinal component of the normalized spin density, $\bar{S}_z$, on the topological charge ℓ of Bessel vortex beams, which has been previously predicted analytically in Ref. 1. According to the notation introduced in the main text, the results refer to $(N, \ell) = (\infty, \pm 1)$

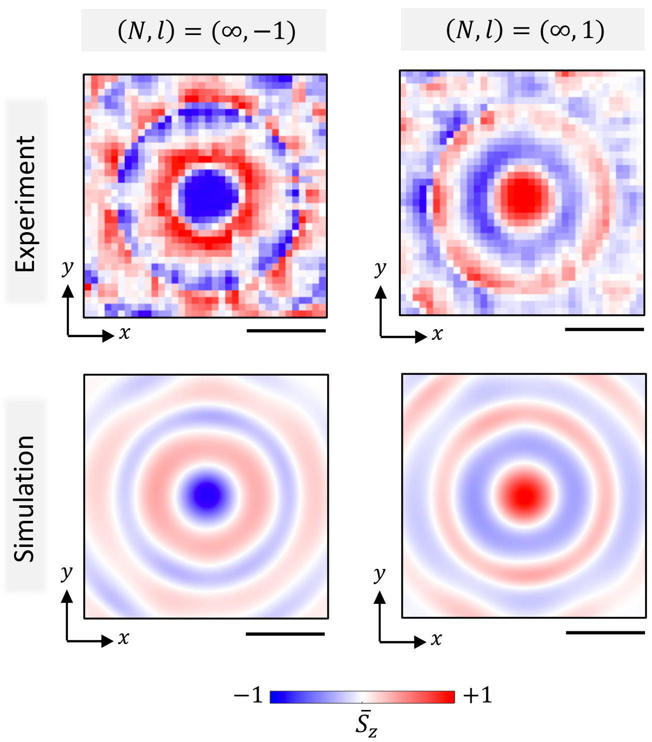

FIG. S1. Experimentally retrieved (top row) and numerically calculated (bottom row) distributions of the longitudinal z component of the normalized spin density $\bar{\mathbf{S}}$ in the transverse (x, y) (at $z = z_{\rm obs}$) for Bessel beams with $\ell = \pm 1$. Scale bars: λ.

2. Skyrmion texture in three-wave interference

Here we show that, for fixed t and z, the direction of the velocity field for a superposition of three plane waves covers the complete sphere when the coordinates (x, y) vary within a given area. The velocity field at this time can then be regarded as a skyrmionic lattice.

The velocity field distribution at, say, $t = 0$ and $z = 0$ (where the field at the origin is maximal) corresponds to the real part of Eq. (2), in this case with $N = 3$ and $\Phi_j = 0$, that is, $\ell = 0$. Recall that, while the experimental implementation used $\ell = -1$, for $N = 3$ a change in Φ_j corresponds to a spatial shift of the pattern and a global phase. Figure 8(a) of the main text shows a simulation based on Eq. (2) of the direction of the velocity field at each point, with color-encoded direction: hue encodes the azimuthal coordinate (longitude) and light-dark encodes the polar coordinate (latitude). The pattern in Fig. 8(a) can be subdivided into cells over which all directions appear only once. This subdivision is not unique, but for convenience we choose aligned horizontal rectangular sections. Note that the vertical limiting lines can be shifted arbitrarily without changing the fact that each direction is covered only once, while the horizontal lines are fixed. (In fact, the vertical boundaries of the third and fourth rows could be shifted by half a period to better match the patterns of the first and second rows, but such change is irrelevant to the covered velocity field directions.) The coverage of the sphere of directions for a Cartesian sampling of one of these cells is shown in Fig. 8(b) and Supplementary Video 1.

The measurements follow the theoretical predictions. Figure 8(c) shows the skyrmionic texture for the measured velocity field at $t = 0$, using the same data over the same area as that in the third panel in Fig. 6(a). The top section (enclosed in a rectangle) approximately corresponds to a cell like those in Fig. 8(a) (with the vertical boundaries shifted). The coverage of directions over the sphere for the measured points is shown in Fig. 8(d) and Supplementary Video 2.

We now discuss how the coverage of the sphere of directions changes with time. At any given time t and distance z, the density of the mapping from the plane (x, y) to the surface of the sphere of directions is characterized by the Skyrme density, defined as

$$\sigma(x, y; z, t) = \frac{1}{4\pi} \hat{\mathbf{u}} \cdot \frac{\partial \hat{\mathbf{u}}}{\partial x} \times \frac{\partial \hat{\mathbf{u}}}{\partial y}, \tag{S1}$$

where

$$\hat{\mathbf{u}} = \frac{\mathrm{Re}\left[\mathbf{v}(\mathbf{r})e^{-i\omega t}\right]}{\left|\mathrm{Re}\left[\mathbf{v}(\mathbf{r})e^{-i\omega t}\right]\right|}. \tag{S2}$$

The integral of the Skyrme density over a unit cell gives the Skyrme number,

$$\Sigma(z, t) = \iint_{\text{unit cell}} \sigma(x, y; z, t)\, dx\, dy, \tag{S3}$$

which equals ± 1 if the sphere is fully covered over the corresponding area, the sign determining the sense in which the coverage takes place.

As Fig. 8 shows, for $t = 0$ and $z = 0$ the coverage is fairly uniform. However, for other times (or equivalently, for other propagation distances z) it can become more irregular, and in fact the sign of the Skyrme number presents abrupt changes. The reason for this can be appreciated from Supplementary Video 3, which shows the evolution of the coverage over a temporal period, as well as the skyrmionic texture. One can see that there are topological transitions at certain times and locations (associated with zeros of the field). The video also shows that the even and odd rows of cells shown in Fig. 8(a) no longer cover each the complete sphere of directions separately; for each some sections are not covered and others are covered twice. However, together such two contiguous cells do cover the complete sphere twice. Note that for $t = mT/6$, where m is an integer and $T = 2\pi/\omega$ is the temporal period of the acoustic wave, the coverage of the sphere is similar to that of $t = 0$, where each cell covers fairly uniformly the whole sphere.

Figure S2 shows the temporal evolution of the Skyrme number averaged over two vertically contiguous cells (see Fig. 8), $\overline{\Sigma}$, both for the theoretical case (black curve) and for the experimental data (blue curve). For the theoretical case the coverage is complete almost at any time, but it switches sign six times per cycle. The experimental counterpart presents similar oscillations, however without exhibiting a perfect square waveform due not only to experimental limitations but also to the coarse sampling that results in a rough estimations of the spatial derivatives and of the integral.

Finally, Fig. S3 shows en enlarged version of the panel (c) of Fig. 8 that allows to better appreciate the details of the velocity field direction distribution.

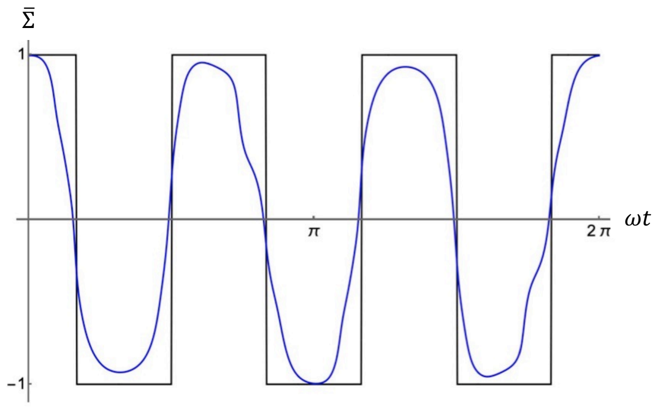

FIG. S2. Skyrme number $\overline{\Sigma}$ averaged over two vertically contiguous cells (see Fig. 8), as a function of time over a wave cycle at fixed z, for the theoretical superposition of three plane waves (black curve) and for the experimental measurements (blue curve).

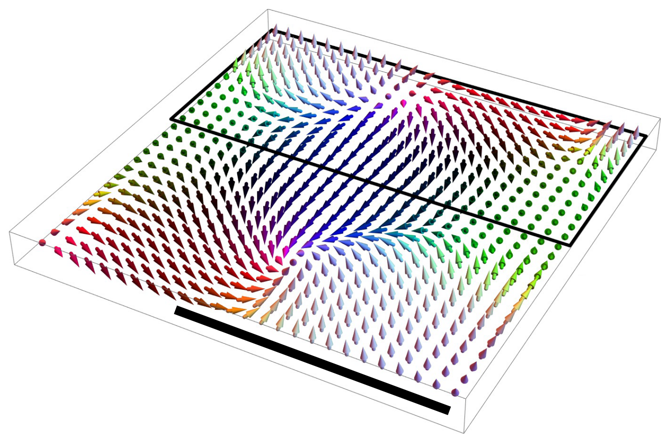

FIG. S3. Enlarged version of Fig. 8(c). We refer to the caption of Fig. 8.

3. Video captions

Video 1. For a theoretical model of three plane waves: (left) coverage of the sphere of directions; (middle) color representation of distribution of directions over the (x, y) plane; (right) skyrmionic texture (at one third of the sampling of the other two parts). In all parts, the color scheme for representing velocity field directions follows the palette at the center of Fig. 8.

Video 2. For the experiment using a triangular grating: (left) coverage of the sphere of directions, where due to the lower sampling a grid of white lines is used to aid visualisation; (middle) color representation of distribution of directions over the (x, y) plane; (right) skyrmionic texture. In all parts, the color scheme for representing velocity field directions follows the palette at the center of Fig. 8., and the sampling corresponds to that of the experimental data.

Video 3. Time evolution of the velocity field directions for a theoretical model of three plane waves. The distributions of points over the spheres at the top and bottom panels on the left column correspond, respectively, to the coverage of velocity field directions of the cells over the first and second (or equivalently third and fourth) rows of any of the two columns of the plane in the top-right panel. The bottom-right panel shows the skyrmionic texture corresponding to the two cells at the top-left of the panel above.

[1] K. Y. Bliokh and F. Nori, "Spin and orbital angular momenta of acoustic beams," Phys. Rev. B **99**, 174310 (2019).